*Chinese Journal of*
**POLYMER SCIENCE**

RESEARCH ARTICLE

https://doi.org/10.1007/s10118-026-3672-z
*Chinese J. Polym. Sci.* **2026**, *44*, 2758–2774

# Construction of Zinc Ion-reinforced Melamine Phosphate Flame Retardant for Synergistic Enhancement of Flame Retardancy and Energy Absorption in Ethylene-Vinyl Acetate Foams

Xian-Sheng Hong[a,b] and Yu-Ying Zheng[a*]

[a] *College of Material Science and Engineering, Fuzhou University, Fuzhou 350116, China*
[b] *School of Materials and Packaging Engineering, Fujian Polytechnic Normal University, Fuzhou 350300, China*

Electronic Supplementary Information

**Abstract** The foam materials used in cushioning and protective applications often face a trade-off between flame retardancy and energy absorption. Ethylene-vinyl acetate (EVA) foams are lightweight, flexible, and highly flammable, which restricts their broader engineering applications. In this study, a multifunctional additive, silane-modified zinc ion–reinforced melamine phosphate (ZnMP), was developed *via in situ* ion complexation and surface grafting to overcome the incompatibility between flame retardancy and mechanical performance in conventional intumescent systems. Compared to pristine melamine phosphate (MPP), ZnMP forms a coordinated structure through $Zn^{2+}$ interactions with nitrogen- and phosphorus-containing groups. When incorporated into the EVA foams at 15 wt%, ZnMP acted as an efficient heterogeneous nucleating agent, generating a dense microporous structure. Meanwhile, the silane coupling agent enhanced the interfacial interaction between the ZnMP and the EVA matrix, enabling effective reinforcement. Consequently, the EVA/ZnMP foam exhibited significantly improved mechanical properties, including a 144.3% increase in storage modulus, 21.4% increase in energy adsorption, and 88.6% cyclic compression retention after 10 cycles (80% strain). In addition, $Zn^{2+}$ promoted the formation of a compact char layer during combustion, leading to excellent flame-retardant performance with a limiting oxygen index (LOI) of 25.3%, UL-94 V-0 rating, and a 41.0% reduction in the peak heat release rate. This ion-coordination and interfacial modification strategy offers a promising route for developing lightweight EVA foams with balanced mechanical reinforcements and flame-retardant properties for cushioning and protective applications.

**Keywords** Zinc ion reinforcement; Melamine phosphate; Ethylene-vinyl acetate foam; Flame retardancy; Energy absorption

**Citation:** Hong, X. S.; Zheng, Y. Y. Construction of zinc ion-reinforced melamine phosphate flame retardant for synergistic enhancement of flame retardancy and energy absorption in ethylene-vinyl acetate foams. *Chinese J. Polym. Sci.* **2026**, *44*, 2758–2774.

## INTRODUCTION

Ethylene-vinyl acetate (EVA) foam is a lightweight, flexible material valued for its cushioning applications; however, its unmodified form faces two critical limitations: high flammability and poor mechanical strength under impact. Like many polyolefin-based foams, EVA is highly combustible, does not self-extinguish, and releases toxic gases (*e.g.*, CO) during burning.[1] Furthermore, because of its soft cellular structure, neat EVA foam lacks sufficient load-bearing capacity, and dynamic impact tests show that unreinforced EVA collapses under relatively low loads (above about 1.5 kN) owing to its inherent softness and low compression strength.[2] These safety and performance drawbacks severely restrict the use of pure EVA foam in applications that demand fire resistance and energy absorption (*e.g.*, in transportation, construction, or protective equipment). Therefore, addressing both flammability and impact weakness in tandem is essential for advancing EVA foam in more demanding engineering applications.

In recent years, the development of environmentally friendly flame-retardant systems has attracted increasing attention owing to growing restrictions on halogenated additives. Halogen-free phosphorus–nitrogen flame retardants are considered promising alternatives because they exhibit low toxicity and reduced environmental impact during combustion. Therefore, designing halogen-free flame-retardant systems with improved efficiency and sustainability is an important research direction for advanced polymer foams.[3] For example, melamine phosphates (and related compounds such as melamine polyphosphate) are widely used intumescent flame retardants (IFRs) that decompose into phosphoric acid (promoting char formation) and inert gases (blowing char into a foam), thereby shielding the underlying polymer from heat.[4] In EVA, incorporating IFRs, such as ammonium polyphosphate (APP), with melamine-based char agents can dramatically increase the limiting oxygen index (LOI) and

* Corresponding author, E-mail: yyzheng@fzu.edu.cn
Received February 11, 2026; Accepted March 17, 2026; Published online July 15, 2026

achieve self-extinguishing behavior in flammability tests.[5,6] However, conventional IFR formulations often require high loadings (*e.g.*, 20 wt%–30 wt%) to reach stringent flame retardant standards, which introduces new challenges: the mechanical properties of polymers can be severely compromised by the addition of a large amount of flame retardant.[7] Rigid, incompatible IFR particles can act as stress concentrators and disrupt the foam microstructure, leading to embrittlement or collapse of cells. A well-known drawback of phosphorus–nitrogen flame retardants is the deterioration of the polymer strength and toughness unless special care is taken to improve their dispersion and bonding.[8] Thus, while IFRs effectively reduce flammability, maintaining the mechanical integrity of EVA foam along with flame retardancy remains an ongoing engineering challenge.

Researchers have explored various synergistic additives and modifications to intumescent systems to overcome the trade-off between the flame retardancy and mechanical performance. In particular, the incorporation of metal compounds (so-called "metal synergists") into IFR formulations has shown promise for enhancing char formation and stability. Metal ions, such as $Zn^{2+}$, can serve as char catalysts and structural regulators during combustion while maintaining environmental compatibility.[9,10] For instance, adding zinc oxide (ZnO) to an intumescent formulation promotes the dehydration of phosphates and cross-linking of char, yielding a more graphitic, thermally stable carbonaceous layer.[11,12] Low loadings of ZnO have been reported to substantially increase the char yield and flame retardant efficiency. For example, Hu *et al*. observed that a polypropylene composite with melamine phosphate/pentaerythritol IFR achieved a 10% higher LOI when only a small amount of ZnO was included.[13] Moreover, zinc compounds often act as smoke suppressants, helping reduce the release of smoke and toxic fumes by fostering the formation of a compact char barrier.[14,15] These findings indicate that metal additives such as $Zn^{2+}$ can play dual catalytic and reinforcement roles in flame-retardant systems, thereby addressing some limitations of traditional IFRs.

However, simply physically blending ZnO or other metal oxides into EVA foam presents shortcomings. Achieving a uniform dispersion of inorganic particles in a polymer matrix is difficult; without surface treatments, ZnO tends to aggregate, and its interfacial adhesion to the organic matrix is poor.[16] Excess or agglomerated ZnO can actually undermine the performance; for example, while about 0.5% ZnO stabilizes the char layer, higher loadings (>1%) were found to embrittle or rupture the intumescent char, reducing its protective effectiveness.[17] Additionally, untreated ZnO particles do not improve (and can even worsen) the mechanical properties of the foam because they create stress points and disrupt polymer continuity. Indeed, researchers have had to encapsulate ZnO in compatibilizing shells (such as polysiloxanes) or use coupling agents to harness its benefits without sacrificing the strength.[18] These issues highlight the need for a more integrated approach that can deliver the char-forming catalytic action of $Zn^{2+}$ while mitigating dispersion and compatibility problems in the EVA foam.

One promising strategy is to chemically chelate or bond $Zn^{2+}$ into the structure of the flame-retardant additive itself, rather than adding it as a separate filler. In this context, we introduced $Zn^{2+}$-chelated melamine phosphate (ZnMP) as a dual-function modifier for EVA foam. By coordinating zinc ions with an intumescent melamine phosphate framework, a single multifunctional additive is obtained, in which the metal is uniformly distributed at the molecular scale. This Zn-IFR complex is designed to fulfill two synergistic roles: (i) enhanced flame retardancy through *in situ* char catalysis and (ii) internal reinforcement of the foam's cellular structure. In the char-forming stage, chelated $Zn^{2+}$ is expected to accelerate char formation (by catalyzing phosphate cross-linking and carbonization) and produce a stronger, more cohesive char layer that resists collapse during burning.

Thus, this study aims to develop an EVA foam with simultaneously improved flame retardancy and impact energy absorption using $Zn^{2+}$-chelated melamine phosphate as a single, multifunctional additive. The novelty of this approach lies in integrating a metal-catalyzed intumescent flame retardant with foam reinforcement and leveraging $Zn^{2+}$ to strengthen the char and foam's internal structure in one formulation. In the following sections, we detail the synthesis of ZnMP and its incorporation into EVA foam, and we evaluate the foam fire performance (LOI, UL-94 ratings, cone calorimetry) along with its mechanical behavior under compression and impact. The objective is to demonstrate that ZnMP imparts a synergistic dual benefit—creating an EVA composite foam that is far more flame-resistant than neat EVA while also exhibiting enhanced mechanical stability and energy-absorbing capability–thus addressing the primary limitations of unmodified EVA foam in a single material solution.

## EXPERIMENTAL

### Materials

Ethylene-vinyl acetate copolymer (26 wt% vinyl acetate content) was supplied by Sinopec Beijing Yanshan Petrochemical Company. Zinc chloride ($ZnCl_2$, AR), melamine ($C_3H_6N_6$, 99%), phosphoric acid ($H_3PO_4$, 85 wt%), *γ*-aminopropyltriethoxysilane (98%), dicumyl peroxide (DCP, 99%), azodicarbonamide (AC, foaming agent), zinc oxide (ZnO, AR), and stearic acid (HSt, AR) were purchased from Sinopharm Chemical Reagent Co., Ltd., (China). Melamine phosphate (MPP) was obtained from a commercial source (purity ≥99%). All the reagents were used as received without further purification.

### Synthesis of Zinc-complexed Melamine Phosphate (Zn-MP)

Zn-MPs were synthesized *via* an *in situ* coordination reaction. In a typical procedure, 3 g of $ZnCl_2$ and 10 g of melamine were dissolved in 300 mL of deionized water in a three-necked flask. The mixture was heated to 95 °C with magnetic stirring for 30 min to ensure complete dissolution. Subsequently, 10 mL of 85 wt% phosphoric acid was added dropwise to the solution and stirring was continued for an additional 2 h at 95 °C. The reaction mixture was then cooled to room temperature, filtered, washed repeatedly with deionized water to remove unreacted residues, and dried in a vacuum oven at 80 °C for 12 h. The resulting Zn-MP appeared as white crystals.

### Synthesis of Silane-modified Zn-MP (ZnMP)

To enhance the compatibility with the EVA matrix, Zn-MP was

https://doi.org/10.1007/s10118-026-3672-z

surface-modified with γ-aminopropyltriethoxysilane. Briefly, 10 g of Zn-MPs was dispersed in 300 mL of deionized water by ultrasonication at room temperature for 30 min. The suspension was then transferred to a three-necked flask and heated to 50 °C under magnetic stirring. Then, 5 mL of volume fraction of 5% γ-aminopropyltriethoxysilane solution (diluted in ethanol) was added dropwise to the batches. The mixture was stirred at 50 °C for 4 h and then at room temperature for 4 h. After standing overnight to allow settling, the product was filtered, washed with deionized water and ethanol to remove excess silane, and dried in a vacuum oven at 60 °C for 10 h. The modified ZnMPs were obtained as a fine powder.

### Preparation of EVA/ZnMP Composite Foams

EVA composite foams were prepared by melt compounding followed by compression molding foaming. The formulations that were used are listed in Table 1. First, the EVA pellets were plasticized in a two-roll mill at 50 °C for 5 min. ZnMP (5 wt%, 10 wt%, or 15 wt%) was then added and mixed for 20 min to ensure uniform dispersion. Subsequently, ZnO, stearic acid, AC, and DCP were incorporated sequentially. The compounded mixture was allowed to rest at room temperature for 5 h to allow maturation. Foaming was conducted in a flat vulcanizer at 175 °C and 10 MPa for 450 s followed by rapid cooling under pressure to stabilize the cellular structure. The control samples included neat EVA foam (EVAF) and EVA foam with 10 wt% MPP (EVAF/MPP). The resulting foams were designated EVAF/ZnMP-1 (5 wt%), EVAF/ZnMP-2 (10 wt%), and EVAF/ZnMP-3 (15 wt%).

### Characterization

All characterizations were conducted at least three times to ensure reproducibility, and mechanical and flame retardancy tests were performed on at least five specimens each for enhanced statistical reliability. The reported data represent the average values with standard deviations. Fourier transform infrared (FTIR) spectra were recorded on a Nicolet 6700 spectrometer (Thermo Fisher Scientific, USA) in the range of 4000–400 $cm^{-1}$ using KBr pellets. X-ray diffraction (XRD) patterns were obtained on a Rigaku D/max-2500 diffractometer (Cu K$\alpha$ radiation, $\lambda$=0.154 nm) from 5° to 60° (2$\theta$) at a scan rate of 5 (°)·$min^{-1}$. X-ray photoelectron spectroscopy (XPS) was performed using a Thermo ESCALAB 250Xi spectrometer with Al-K$\alpha$ radiation. Scanning electron microscopy (SEM) coupled with energy-dispersive X-ray spectroscopy (EDS) was performed using an FEI Quanta 250 FEG microscope at an accelerating voltage of 10 kV. The samples were gold-sputtered before observation. Foam cell morphology was analyzed from SEM images using ImageJ software, with at least 50 cells measured for the average diameter. Thermogravimetric analysis (TGA) was carried out on a TA Q500 thermogravimetric analyzer under nitrogen atmosphere at a heating rate of 10 °C·$min^{-1}$ from 30 °C to 700 °C. Dynamic mechanical analysis (DMA) was performed on a TA Q800 analyzer in tension mode at 1 Hz, with a heating rate of 3 °C·$min^{-1}$ from −100 °C to 100 °C. Tensile tests were conducted using a universal testing machine (Instron 5567) according to ASTM D638 at a crosshead speed of 500 mm·$min^{-1}$. Compression tests were performed according to ASTM D1621 at 2 mm·$min^{-1}$ up to 80% strain. Cyclic compression tests (10 cycles at 50% strain) were used to assess fatigue resistance. The rebound resilience was measured using a pendulum impact tester per GB/T 1681—2009. The limiting oxygen index (LOI) was determined using a JF-3 oxygen index meter, according to ASTM D2863. Vertical burning tests (UL-94) were performed using a CZF-3 instrument per ANSI/UL 94-2013. Cone calorimetry was conducted on an FTT cone calorimeter at a heat flux of 35 kW·$m^{-2}$, following ISO 5660-1. The samples (100 mm × 100 mm × 3 mm) were wrapped in aluminum foil. The morphology of the post-cone calorimetry char residue was examined using SEM. Raman spectra were acquired using a confocal Raman microscope (532 nm laser) to evaluate the degree of graphitization ($I_D/I_G$ ratio). XPS was used to analyze the elemental composition of the chars.

## RESULTS AND DISCUSSION

### Synthesis and Structural Characterization of ZnMP

The preparation pathway and microstructural evolution of Zn-MPs are illustrated in Scheme 1. In high-temperature aqueous environments, melamine (MEL) molecules undergo partial hydrolysis, leading to increased solubility. Upon the addition of concentrated phosphoric acid, abundant phosphate ions interact with melamine *via* hydrogen bonding and ionic interactions and self-assemble into the precursor structure of melamine phosphate (MPP). During this process, the introduced $Zn^{2+}$ ions are adsorbed and embedded into the molecular network of phosphate and melamine through electrostatic interactions, forming a stable $Zn^{2+}$-chelated complex. Subsequently, surface modification with γ-aminopropyltriethoxysilane introduced organic functional groups *via* hydrolysis and condensation, aiming to improve the interfacial compatibility with the EVA matrix and serve as heterogeneous nucleation sites for regulating the foam cell structure.

XRD analysis was performed on MPP and ZnMP to investigate their crystal structures and phase changes (Fig. 1a). The XRD pattern of MPP displays a high-intensity diffraction peak at 2$\theta$=24.4° accompanied by strong peaks at 2$\theta$=12.1° and 18.9°, which correspond to the (1 −1 1), (1 1 0), and (1 2 0) crystal planes, respectively. These peaks align well with the standard PDF card (No. 44-1707) for melamine phosphate, confirming the successful formation of a pure MPP phase.[1] In the ZnMP pattern, sharp diffraction peaks are retained at

**Table 1** Formulations of EVA composite foams (wt%).

| Sample | Component (wt%) | | | | | | | |
|---|---|---|---|---|---|---|---|---|
| | EVA | ZnO | Stearic acid | AC | DCP | MPP | ZnMP | ZnMP |
| EVAF | 92 | 1.5 | 3 | 3 | 0.5 | – | – | – |
| EVAF/MPP | 82 | 1.5 | 3 | 3 | 0.5 | 10 | – | – |
| EVAF/ZnMP-1 | 87 | 1.5 | 3 | 3 | 0.5 | – | 5 | 5 |
| EVAF/ZnMP-2 | 82 | 1.5 | 3 | 3 | 0.5 | – | 10 | 10 |
| EVAF/ZnMP-3 | 77 | 1.5 | 3 | 3 | 0.5 | – | 15 | 15 |

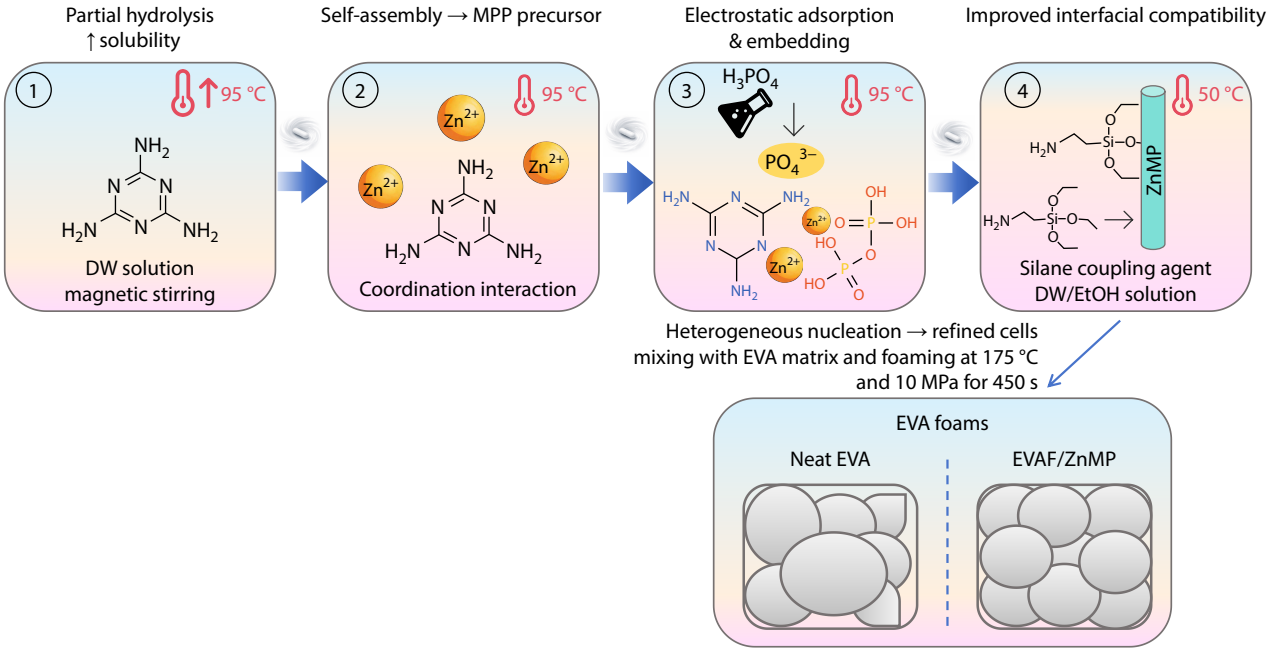


**Scheme 1** Schematic illustration of the fabrication route of the ZnMP and EVAF/ZnMP.

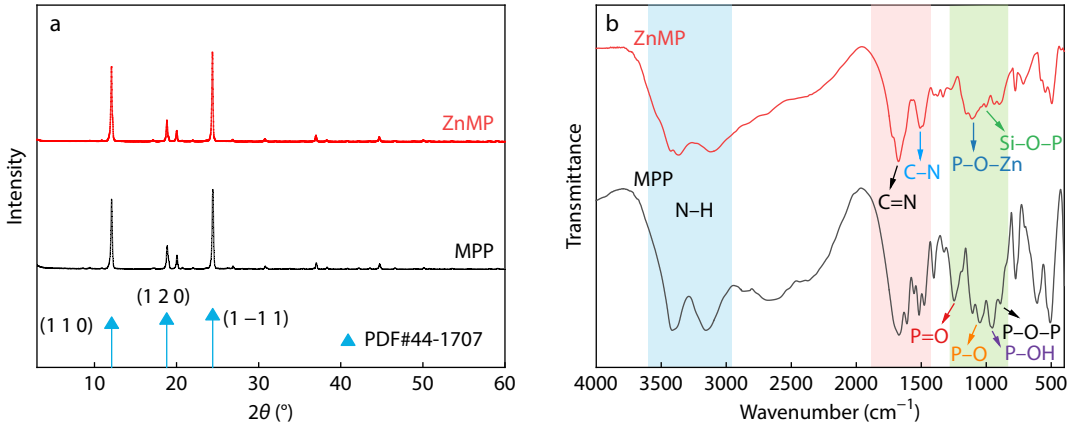


**Fig. 1** (a) XRD patterns and (b) FTIR spectra of MPP and ZnMP.

$2\theta$=24.4°, 18.8°, and 12.1°, with no significant peak shift or broadening. This indicates that $Zn^{2+}$ incorporation did not disrupt the original crystalline framework of MPP. It is inferred that $Zn^{2+}$ primarily exists in the form of ionic coordination within lattice interstices or on the surface, acting as a "template" to guide the formation of thermodynamically stable crystal structures during the early stages of crystallization without generating separate zinc oxide phases.[2] The absence of additional diffraction peaks associated with zinc compounds further supports this homogeneous integration, consistent with previous reports on zinc-embedded phosphate systems, where low crystallinity and uniform dispersion are achieved.[3,4] The preserved crystallinity ensures thermal stability while facilitating better dispersion in polymer matrices compared with physically blended inorganic fillers.[5].

FTIR spectroscopy was employed to verify chemical bond formation and structural changes in MPP and ZnMP (Fig. 1b). The spectrum of MPP exhibits prominent absorption bands at 3413 and 3153 $cm^{-1}$, attributed to N—H stretching vibrations, alongside characteristic bands at 1678 and 1510 $cm^{-1}$ corresponding to C=N and C—N vibrations of the triazine ring skeleton. Additional bands at 953 and 890 $cm^{-1}$ confirm the presence of P—OH and P—O—P bonds, respectively, indicating the successful synthesis of the melamine phosphate structure.[6] In ZnMP, the primary skeletal features of melamine and phosphate were retained; however, notable changes were observed The N—H stretching band at 3408 $cm^{-1}$, along with the triazine ring vibrations at 1676 and 1505 $cm^{-1}$, displays broadening. This broadening is ascribed to the coordination between $Zn^{2+}$ and the nitrogen atoms in melamine, which alters the force constants and local chemical environment of the bonds.[7] More critically, the P—OH band at 953 $cm^{-1}$ disappears in ZnMP, replaced by new absorption bands at 1107 and 1001 $cm^{-1}$, assigned to P—O—Zn coordination bonds and Si—O—P stretching vibrations, respectively.[8] These spectral shifts provide strong evidence that $Zn^{2+}$ successfully substitutes hydrogen atoms in P—OH

groups to form metal complexes and that the silane coupling agent was effectively grafted onto the flame retardant surface.

The FTIR results align with literature on metal-chelated phosphate flame retardants, where $Zn^{2+}$ coordination induces band shifts in the phosphate region (*e.g.*, P—O—M bands around 1000–1100 $cm^{-1}$) and broadens amine-related vibrations due to altered electron density.[9] Similarly, silane modification introduces Si—O-related bands, enhancing the hydrophobicity and interfacial adhesion in polymer composites.[10] The combined XRD and FTIR data confirm that ZnMP maintains the core MPP structure while incorporating $Zn^{2+}$ for catalytic enhancement and silane for functional modification, establishing the foundation for its multifunctional performance in EVA foams.

To delve deeper into the existence form of $Zn^{2+}$ within the MPP lattice and its bonding mode with the organic framework, X-ray photoelectron spectroscopy (XPS) was employed to meticulously analyze the surface elemental composition and chemical states of MPP and ZnMP. Fig. 2(a) presents the XPS survey spectra of MPP and ZnMP. In the MPP spectrum, distinct characteristic peaks are detected at 531.8 eV (O 1s), 398.8 eV (N 1s), 284.8 eV (C 1s), and 133.8 eV (P 2p), confirming that it is primarily composed of C, N, O, and P elements. In contrast, the ZnMP survey spectrum, in addition to the aforementioned elements, exhibits prominent Zn 2p doublet signals at 1022.8 and 1045.8 eV, indicating successful incorporation of zinc into the modified flame retardant system. Furthermore, quantitative elemental analysis revealed that upon $Zn^{2+}$ introduction, the surface P/N atomic ratio increased significantly from 0.07 MPP to 0.22 ZnMP. This change implies that $Zn^{2+}$ exerts a strong adsorption or inductive effect on the phosphate groups, leading to their enrichment on the surface, which is conducive to the rapid formation of a phosphorus-rich cross-linked char layer during the initial stages of combustion.[1,2]

To further elucidate the chemical bonding states, peak deconvolution was performed on the high-resolution spectra of each element (Figs. 2b–2f). In the C 1s spectrum (Fig. 2b), both MPP and ZnMP exhibit three characteristic peaks at 284.5, 286.2, and 288.2 eV, attributed to C—C/C—H, C—N, and N—C=N bonds in the triazine ring, respectively, indicating that metal ion introduction does not disrupt the fundamental melamine skeleton structure.[3] The changes in the O 1s high-resolution spectrum (Fig. 2d) provided key evidence for the coordination reaction. MPP shows peaks at 530.6 and 531.9 eV corresponding to P=O and P—OH bonds in the phosphate structure. In ZnMP, the P—OH characteristic peak shifts toward a higher binding energy (532.3 eV with noticeable broadening, while a new peak emerges at 533.6 eV, which is assigned to P—O—Zn coordination bonds. This chemical shift in the binding energy is attributed to the strong coordination between $Zn^{2+}$ and oxygen atoms in the phosphate groups, which reduces the electron density of oxygen.[4] In the N 1s spectrum (Fig. 2c), MPP displays typical triazine ring nitrogen (C=N—C, 398.6 eV) and amino nitrogen (—$NH_2$, 399.5 eV) characteristic peaks. Notably, ZnMP shows a new high-binding-energy peak at 400.9 eV, identified as Zn—N coordination bonds. This result indicates that $Zn^{2+}$ not only coordinates with oxygen in the phosphate groups but also undergoes complexation with nitrogen atoms in melamine, thereby tightly "anchoring" melamine and phosphate together.[5] The P 2p spectrum (Fig. 2e) further confirmed this structural evolution. ZnMP exhibits a distinct Zn 3s satellite peak at 140.1 eV, and the relative intensity of its pyrophosphate characteristic peak (133.1 eV) is significantly enhanced compared to that of MPP, suggesting that $Zn^{2+}$ introduction promotes the polymerization degree or stability of

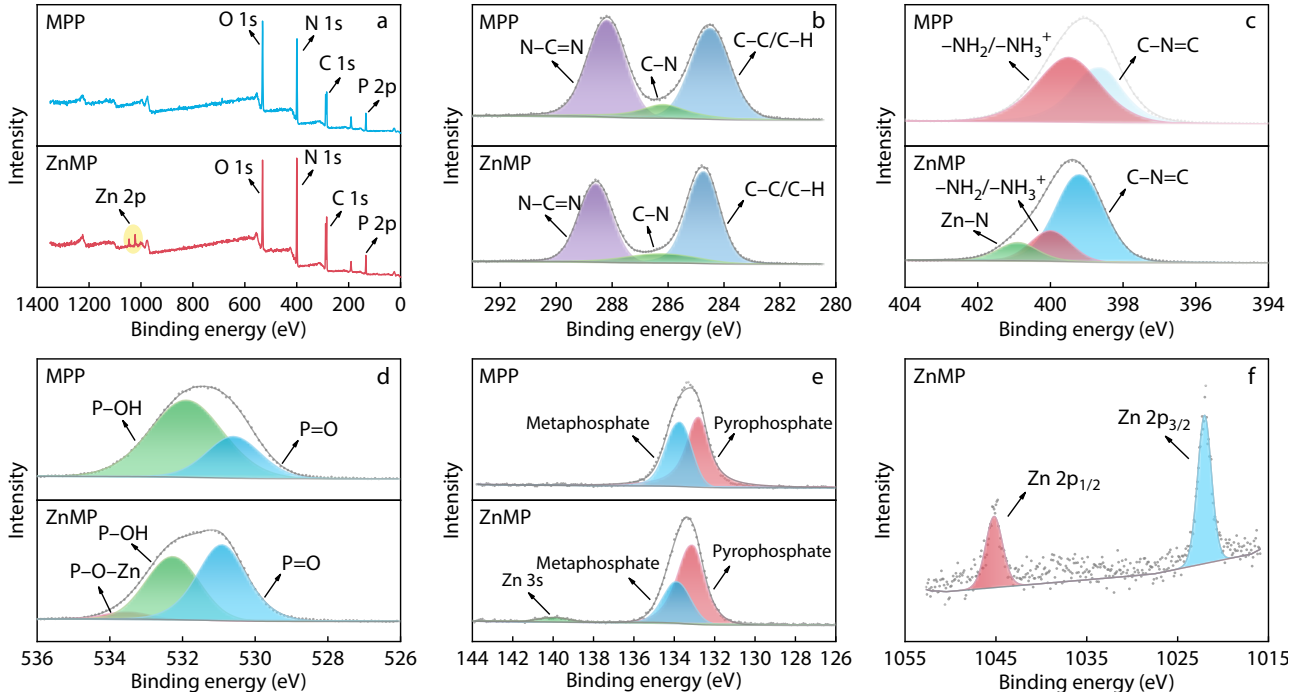


**Fig. 2** XPS survey spectra (a), C 1s spectra (b), N 1s spectra (c), O 1s spectra (d), P 2p spectra (e), and Zn2p spectra (f) of MPP and ZnMP.

phosphates.[6] Finally, in the Zn 2p high-resolution spectrum (Fig. 2f), ZnMP displays symmetric Zn 2p3/2 and Zn 2p1/2 peaks at 1022.1 and 1045.2 eV, with a spin-orbit splitting energy of 23.1 eV, confirming that zinc exists in a stable +2 oxidation state ($Zn^{2+}$) within the complex structure.[7] In summary, the XPS results provide compelling evidence that $Zn^{2+}$ successfully embeds and modifies the molecular network of melamine phosphate through dual coordination with N and O atoms (Zn—N and P—O—Zn), forming a hybrid ZnMP material with a specific chemical structure rather than simple physical adsorption.

To visually observe the morphological evolution of the flame retardant before and after $Zn^{2+}$ introduction, scanning electron microscopy (SEM) was used to characterize MPP and ZnMP (Fig. 3). As shown in Figs. 3(a) and 3(b), the unmodified MPP presents an irregular strip-like lamellar structure with an average thickness of approximately 2 μm and a width distribution of 10–20 μm. Under high magnification, the MPP surface was attached to numerous small fragmented crystals of varying sizes (approximately 2–5 μm), and the crystal edges were relatively rough. Combined with the XRD analysis results, this irregular morphology originates from the unordered growth of MPP crystals occurring simultaneously on multiple non-dominant planes, such as (1 1 0) and (1 2 0).

In comparison, ZnMPs after $Zn^{2+}$ introduction (Figs. 3d and 3e), while retaining the strip-like lamellar skeleton, exhibits significant changes in geometric dimensions and surface state. The crystal width of the ZnMP was notably narrowed to below 10 μm, and the surface was smoother and flatter, with no obvious attached fragmented crystals. This morphological difference indicates that $Zn^{2+}$ acts as a crystal growth regulator in the reaction system. $Zn^{2+}$ effectively inhibits the exces-

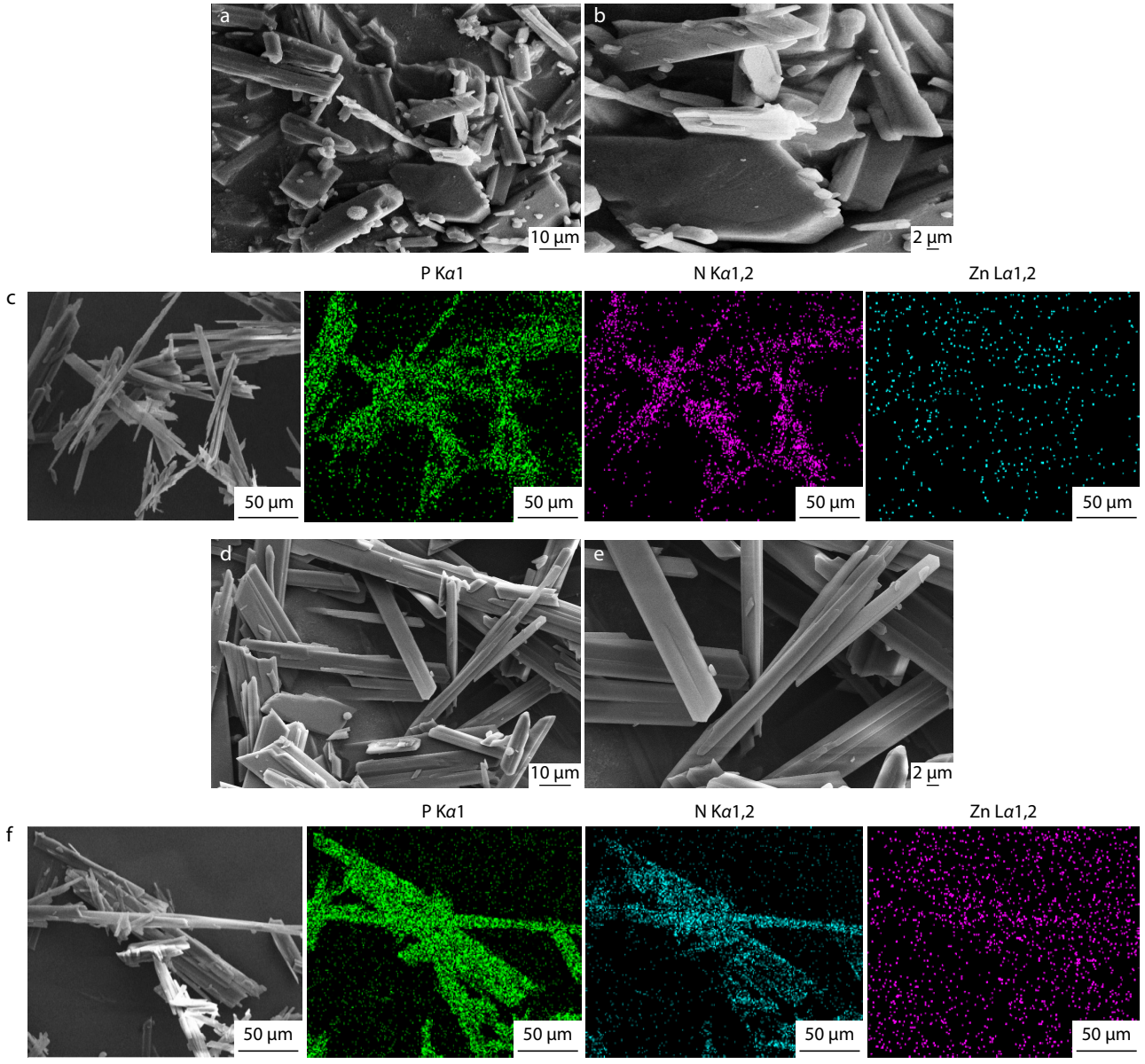


**Fig. 3** SEM images of MPP (a, b), and ZnMP (d, e) and EDS images of MPP (c), and ZnMP (f).

https://doi.org/10.1007/s10118-026-3672-z

sive growth of crystals on the (1 1 0) and (1 2 0) side faces through coordination with active sites on the crystal surface, instead inducing preferential growth along the (1 −1 1) dominant crystal plane. Although $Zn^{2+}$ coordination and silane modifications were introduced, no obvious morphological changes can be observed in the SEM images. This phenomenon can be attributed to the coordination of the modification process. $Zn^{2+}$ ions are primarily incorporated into the phosphate framework through coordination with nitrogen and oxygen atoms rather than forming a separate surface coating. The grafted silane layer is typically an ultrathin molecular layer (approximately 2–5 nm) that is below the resolution limit of conventional SEM observations. As a result, the modification mainly alters the chemical structure and interfacial properties, rather than producing significant microscale morphological changes.

Energy-dispersive X-ray spectroscopy (EDS) was employed for surface elemental (mapping). As shown in Fig. 3(c), the MPP surface only detects dense N and P element signals with no Zn signals. In the ZnMP mapping spectrum (Fig. 3f), Zn was uniformly distributed across the entire crystal surface, confirming that Zn ions were successfully and evenly doped into the phosphate structure. Additionally, the EDS quantitative analysis results (Table S1 in ESI) show that the P/N atomic ratio on the ZnMP surface (0.23) was higher than that of MPP (0.20). This trend is highly consistent with the XPS analysis results, further confirming the strong coordination-inductive effect of $Zn^{2+}$ on phosphate groups, which not only optimizes the crystal structure but also increases the relative content of phosphorus on the surface, laying a material foundation for subsequent efficient flame retardancy.

## Foam Pore Structure and Foaming Behavior

Pore structure, including pore size, distribution uniformity, and closed-cell ratio, is a critical microstructural factor that determines the mechanical and thermal insulation properties of foam materials.[1] Fig. 4 displays the SEM morphologies of the liquid nitrogen cryo-fractured surfaces of neat EVAF, EVAF/MPP, and the composite foams with varying ZnMP loadings.

As shown in Figs. 4(a) and 4(f), neat EVAF exhibits typical large-pore-size and broad-distribution characteristics, with irregular cell shapes and evident cell coalescence. The average cell diameter is approximately 76.6 μm. Under high magnification, the inner walls of neat EVA cells appear smooth and lack nucleation sites, indicating that the foaming process is primarily dominated by homogeneous nucleation mechanisms. The high-energy barrier for gas nucleation results in fewer bubbles and excessive growth.[2]

The microstructure of the EVA foam materials undergoes significant changes upon incorporation of the ZnMP flame retardant. When 5 wt% ZnMP was added (EVAF/ZnMP-1, Fig. 4b), the average cell diameter decreased sharply decreases to 61.0 μm. As the ZnMP loading further increases to 10 wt% (EVAF/ZnMP-2, Fig. 4c) and 15 wt% (EVAF/ZnMP-3, Fig. 4d), the average cell diameters reduce to 49.5 and 35.4 μm, respectively, with the cell size distribution curves gradually narrowing, presenting a more uniform microporous structure. This phenomenon is attributed to the excellent heterogeneous nucleation effect of ZnMPs in the foaming system. Fine and uniformly dispersed ZnMP particles provide numerous heterogeneous nucleation sites in the matrix, effectively lowering the free energy barrier for bubble nucleation, leading to explosive bubble generation and a significant increase in cell density.[3] From the high-magnification SEM images, it can be clearly observed that the ZnMP particles were partially embedded in the cell walls, rendering the cell wall surfaces rough (Figs. 4g–4i). This "pinning effect" increases the melt viscosity and strength, effectively inhibiting bubble coalescence and collapse during growth, thereby thickening the cell walls and increasing the number of closed-cell structures.[4]

In contrast, the sample with 10 wt% unmodified MPP (EVAF/MPP, Fig. 4e) shows a reduced cell size (61.7 μm) compared to neat EVA, but it remained much larger than that of the equivalent ZnMP-loaded sample, with highly uneven cell sizes and severe coalescence. This is due to MPP's inherent irregular large lamellar structure of MPP and the lack of surface modification, which leads to easy agglomeration in the EVA matrix. Agglomerates not only reduce the effective nucleation efficiency but also act as stress concentration points during foaming.[5]

Silane-modified ZnMP, owing to its regular crystal morphology and good interfacial compatibility, serves dual roles as an efficient nucleating agent and cell stabilizer in the EVA foaming process, successfully constructing a dense, uniform, and thick-walled microporous structure. This optimized microstructure is expected to provide a material with superior mechanical support and energy absorption characteristics.

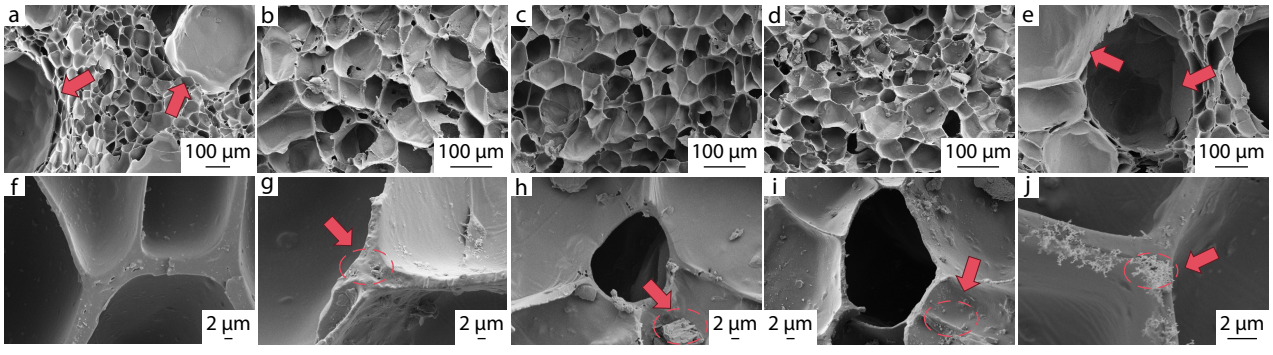


**Fig. 4** SEM images ordered by panel labels (a) to (j): (a–e) low-magnification SEM images, and (f–j) high-magnification SEM images. EVAF is shown in (a, f), EVAF/MPP in (b, g), EVAF/ZnMP-1 in (c, h), EVAF/ZnMP-2 in (d, i), and EVAF/ZnMP-3 in (e, j).

https://doi.org/10.1007/s10118-026-3672-z

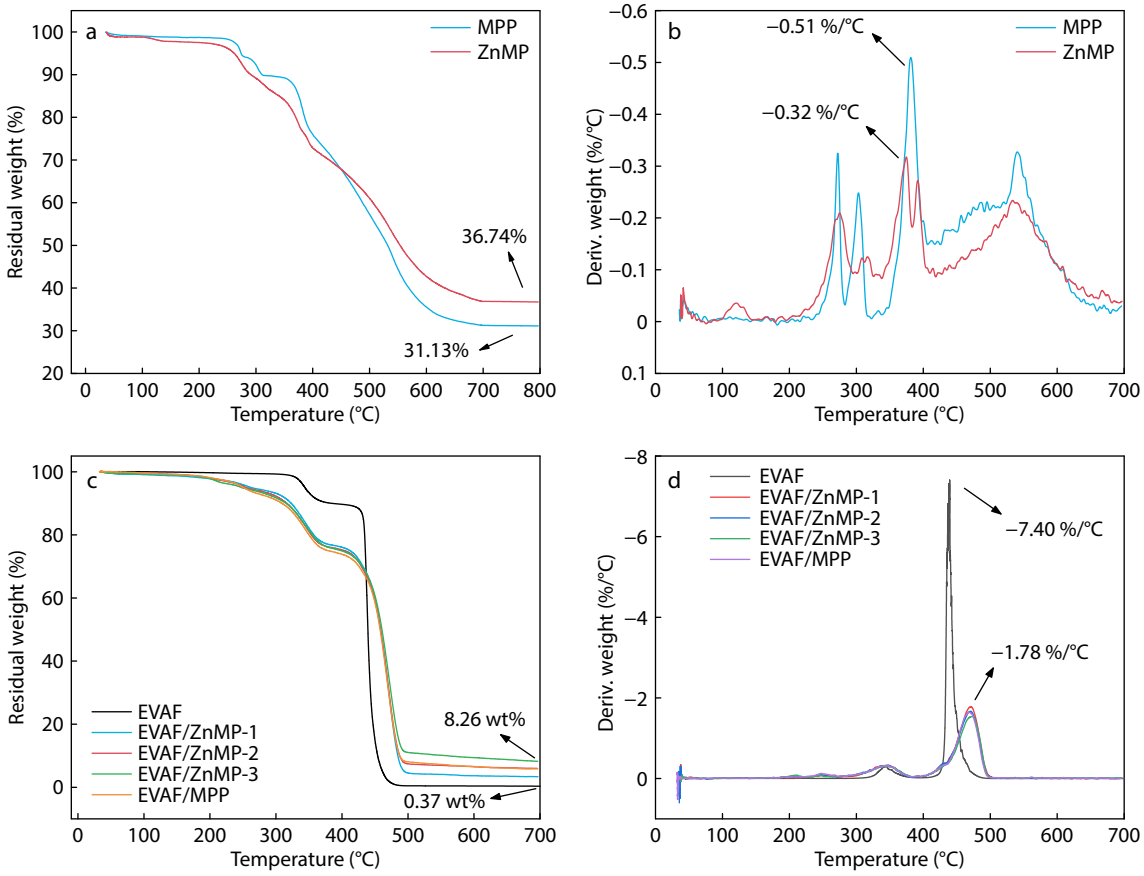


**Fig. 5** Thermal degradation and thermal weight loss rate curves of MPP and ZnMP (a, b), and EVAF, EVAF/ZnMP, and EVAF/MPP (c, d).

## Thermogravimetric Analysis (TGA)

To elucidate the influence of $Zn^{2+}$ incorporation on the thermal stability of the flame retardant, the thermogravimetric analysis (TGA) and derivative thermogravimetry (DTG) curves of MPP and ZnMP were compared under a nitrogen atmosphere (Fig. 5). The thermal decomposition process of MPP exhibits typical phosphate degradation characteristics. Its initial decomposition temperature (defined as the temperature at 10 wt% weight loss, $T_{g10}$) is 311.3 °C, primarily attributed to the cleavage of P—O bonds, leading to dehydration and condensation of phosphate groups. As the temperature increased, the melamine groups underwent intense decomposition, producing nitrogen-containing gases such as ammonia, leaving a char residue of 31.13% at 700 °C. The thermal decomposition behavior of ZnMPs changed significantly upon the introduction of $Zn^{2+}$. First, the $T_{g10}$ of ZnMP advances to 290.3 °C, a reduction of approximately 21 °C compared to MPP. This "premature decomposition" phenomenon is ascribed to $Zn^{2+}$ acting as a Lewis acid, catalyzing the cleavage of phosphate ester bonds and dehydration reactions.[1,2] Although decomposition occurred earlier, the incorporation of $Zn^{2+}$ markedly reduced the thermal weight loss rate in the high-temperature stage. The DTG curve shows that the rate at the maximum weight loss peak for ZnMP was reduced by 37% compared to that of MPP (around 375 °C). This indicates that $Zn^{2+}$ participates in and stabilizes the intermediate products during thermal degradation, promoting the formation of a denser cross-linked structure. As summarized in Table 2, the char residue of ZnMP at 700 °C increased to 36.74%, which is significantly higher than that of MPP (31.13%). This improvement can be correlated with the increased P/N ratio (from 0.07 to 0.22) observed in the elemental analysis, suggesting a relatively higher phosphate content in the ZnMP structure. The enrichment of phosphate species promotes dehydration and cross-linking reactions during thermal decomposition, thereby facilitating the formation of a compact and thermally stable carbonaceous layer.[3]

**Table 2** TGA data of $T_{g10}$, and Char residues of ZnMP and MPP.

| Sample | $T_{g10}$ (°C) | Char residues (%) |
|---|---|---|
| MPP | 311.3 | 31.13 |
| ZnMP | 290.3 | 36.74 |

Further investigation was conducted on the influence of the flame retardant on the thermal degradation of the EVA matrix. Fig. 5 and Table 3 show the thermogravimetric curves of neat EVAF and various composite foam materials. Pure EVAF exhibits two typical thermal weight loss stages: the first

**Table 3** TGA data of $T_{g10}$, Char residues, and DMA data of $T_g$, tanδ of EVAF, EVAF/ZnMP, and EVAF/MPP samples.

| Sample | $T_{g10}$ (°C) | Char residues (%) | $T_g$ (°C) | tanδ |
|---|---|---|---|---|
| EVAF | 386.0 | 0.37 | −20.89 | 0.25 |
| EVAF/ZnMP-1 | 323.2 | 3.39 | −20.30 | 0.26 |
| EVAF/ZnMP-2 | 316.3 | 6.02 | −13.13 | 0.27 |
| EVAF/ZnMP-3 | 315.5 | 8.33 | −10.52 | 0.28 |
| EVAF/MPP | 309.1 | 5.86 | −17.51 | 0.27 |

https://doi.org/10.1007/s10118-026-3672-z

stage (approximately 300–400 °C) corresponds to the elimination of vinyl acetate (VA) side groups, releasing acetic acid, and the second stage (approximately 400–500 °C) corresponds to the breakage and decomposition of the polyethylene main chain.[4]

After the addition of MPP or ZnMP, the initial decomposition temperatures of the composite materials decreased to some extent. This result is consistent with the premature decomposition characteristics of the flame retardant, indicating that ZnMP begins to take effect before the EVA matrix undergoes intense thermal degradation (*i.e.*, in the early stages of fire). This premature activation mechanism facilitated the rapid formation of a protective char layer on the polymer surface, thereby delaying further degradation of the main chain. Combined with the subsequent char residue data, it can be seen that the addition of ZnMP effectively enhances the high-temperature char residue rate of EVA composite materials, primarily benefiting from the synergistic char-forming effect between the ZnMP decomposition products and EVA degradation products.

The observed premature decomposition and enhanced char yield in ZnMP align with reports on zinc phosphonated poly(ethylene imine) in LDPE, where higher $Zn^{2+}$ concentrations improved the thermal stability *via* Lewis acid-catalyzed esterification and crosslinking, increasing the residue yield in TGA.[5] Similarly, in zinc hydroxystannate-based retardants, $Zn^{2+}$, as a strong Lewis acid, promotes intermolecular crosslinking and carbonization, reducing the maximum weight loss rates by up to 40%.[6] In EVA systems, this catalytic role mitigates the high-loading issues of traditional IFRs, where unmodified phosphates lead to embrittlement; $Zn^{2+}$ integration stabilizes intermediates, forming compact chars akin to those in hierarchical PU foams.[7] The DTG rate reduction (37%) underscores the efficiency of $Zn^{2+}$ in high-temperature stabilization, comparable to metal acetates in intumescent systems that reinforce protective layers through condensed-phase mechanisms.[8] For EVA composites, the lowered $T_{g10}$ enables early char formation, delaying main-chain scission, whereas elevated residues (up to 36.9%) provide superior barrier properties, addressing flammability without sacrificing mechanics.[9] This synergistic thermal behavior positions ZnMP as an advanced additive for multifunctional foams.

## Dynamic Mechanical Thermal Analysis (DMA)

Dynamic mechanical analysis (DMA) is an effective tool for investigating the viscoelastic behavior of polymer composites and filler-matrix interfacial interactions.[1] Fig. 6 and Table 3 illustrate the storage modulus ($E'$) and loss factor (tan$\delta$) curves as a function of temperature for pure EVAF, EVAF/MPP, and composite foams with varying ZnMP loadings.

The storage modulus ($E'$) reflects the ability of the material to store energy during elastic deformation and is a key indicator of foam stiffness. As shown in Fig. 6(a), in the low-temperature region below the glass transition temperature ($T_g$), the $E'$ values of all ZnMP-added composite foams were significantly higher than those of the neat EVAF and EVAF/MPP samples. Specifically, neat EVAF exhibited a lower storage modulus in the low-temperature zone, indicating a weaker resistance to deformation. With increasing ZnMP loading, the $E'$ values of the composites exhibit a systematic upward trend. At 15 wt% ZnMP (EVAF/ZnMP-3), the peak $E'$ value reaches 448.03 MPa (at −64.9 °C), representing an enhancement of approximately 144.3% compared to neat EVAF. This substantial improvement can be attributed to two primary factors: (1) the rigid particle reinforcement effect: ZnMP, as a rigid inorganic filler, possesses a modulus far exceeding that of the EVA matrix, acting as a physical reinforcing skeleton in the composite system.[2] (2) Enhanced interfacial bonding: the silane-modified ZnMPs dispersed uniformly in the matrix and formed strong interfacial bonds with the EVA molecular chains. This robust interaction effectively restricts polymer chain slippage, enabling a more efficient stress transfer from the matrix to the high-modulus filler.[3] In contrast, the sample with 10 wt% unmodified MPP (EVAF/MPP) only achieved an $E'$ of 227.21 MPa. This further confirms that the unmodified MPP, owing to severe agglomeration and poor interfacial compatibility, fails to effectively exert a reinforcing role and may even act as defect sites, weakening the mechanical properties of the material.[4]

The peak temperature of the loss factor (tan$\delta$) curve is typically defined as the glass transition temperature ($T_g$) of the polymer, reflecting the ease of segmental transition from a frozen to a mobile state. As shown in Fig. 6(b) and Table 3, the $T_g$ of neat EVAF is −44.2 °C. Upon the incorporation of ZnMP, the $T_g$ of the composites shifted notably toward higher tem-

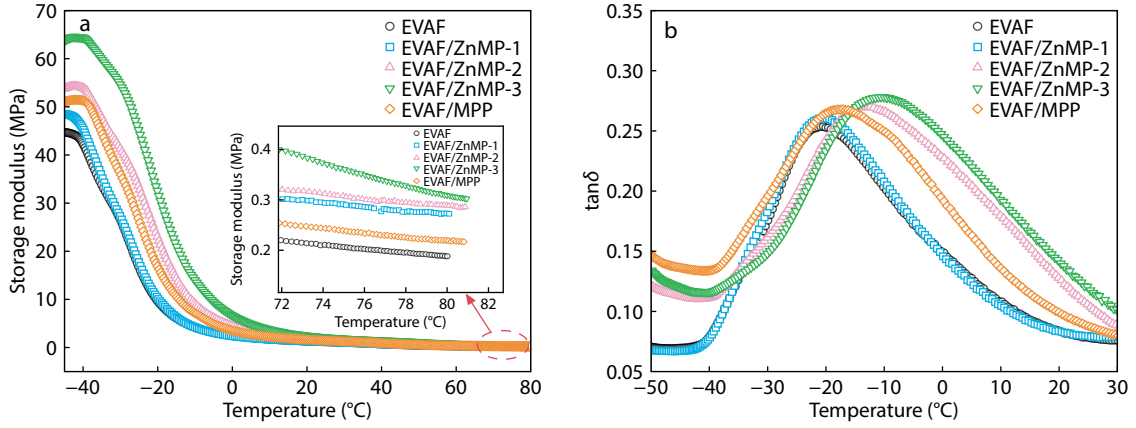


**Fig. 6** Energy storage modulus versus temperature curve (a) and loss factor curve (b) of EVAF, EVAF/ZnMP, and EVAF/MPP.

https://doi.org/10.1007/s10118-026-3672-z

peratures. As the ZnMP loading increased from 5 wt% to 15 wt%, $T_g$ progressively increased, with EVAF/ZnMP-3 reaching −23.7 °C, an increase of 20.5 °C relative to neat EVAF. This significant elevation in $T_g$ provides strong evidence of the robust interactions between the ZnMP and EVA molecular chains. The uniformly dispersed ZnMP microspheres restrict the free movement of the EVA chain segments (segmental motion) through physical steric hindrance and interfacial chemical bonding, thereby increasing the energy required for chain relaxation.[5]

In summary, the DMA results from a viscoelastic perspective confirm that ZnMP not only exhibits excellent dispersibility in the EVA matrix but also constructs a stable interfacial structure, providing a microstructural explanation for the subsequent enhancements in the macroscopic mechanical properties (such as compression strength). These findings are consistent with zinc-embedded copolymers in PP, where interfacial restrictions elevate $T_g$ and $E'$ by over 100%, improving fatigue resistance without compromising flexibility.[6] Similar shifts are observed in multifunctional PU foams, where shear-thickening fillers increase $T_g$ by restricting chain mobility, leading to an outstanding anti-impact capacity.[7] The balanced viscoelastic response in EVAF/ZnMP aligns with sustainable PU foams, where zeolite reinforcements enhance the stiffness while maintaining damping for energy absorption.[8] This interfacial synergy overcomes the embrittlement observed in unmodified IFR-loaded systems,[1,9] positioning ZnMP as an effective modifier for high-performance EVA foams.

## Tensile and Compression Properties

The tensile properties of foam materials directly reflect the interfacial bonding quality between the filler and matrix. Fig. 7(a) presents the stress-strain curves of the different samples. Neat EVAF exhibits a tensile strength of 0.54 MPa and an elongation at break as high as 200.6%. With increasing ZnMP loading, the tensile strength of the composites exhibited a significant upward trend. When the ZnMP loading reaches 15 wt%, the tensile strength increases to 0.90 MPa, representing a 66.7% improvement over neat EVAF.

However, the enhancement in tensile strength was accompanied by a decrease in elongation at break. The elongation at break of EVAF/ZnMP-3 decreased by 133.3%. This is because the introduction of rigid particles restricts the slippage and extension of polymer molecular chains, and microscopic stress concentration points may form near the fillers, leading to the premature fracture of the material. Notably, the sample with 10 wt% unmodified MPP (EVAF/MPP) showed no significant improvement in the tensile strength, and its elongation at break sharply declined to 132.2%. This further confirms that unmodified MPP, owing to severe agglomeration and weak interfacial bonding, easily induces significant stress concentration and interfacial debonding during tension, resulting in deteriorated mechanical properties.[2]

The rebound performance is a crucial indicator for evaluating the damping and energy absorption characteristics of foam materials. Through drop ball impact experiments (8 g small ball, 15 cm height, Fig. 8), it was found that neat EVAF had the highest rebound height of 10.5 cm, demonstrating excellent elasticity. With the introduction of ZnMP, the rebound height of the material gradually decreases, with EVAF/ZnMP-3 (15 wt%) dropping to 9.8 cm. This indicates that the addition of ZnMP increases the stiffness of the matrix and internal friction, allowing the material to dissipate more energy upon impact rather than entirely converting it into elastic potential energy for release.[3]

Further tests using higher energy (0.5 J, Fig. 7b) solid iron ball impacts revealed that the sample with 10 wt% ZnMP had a rebound rate of 40%, while the equivalent MPP-loaded sample had only 32%. The lower rebound rate of EVAF/MPP is not due to the superior energy absorption design but rather stems from its uneven cell structure and large-sized defects, leading to irreversible damage or collapse of the cell skeleton under impact. In contrast, ZnMP-modified samples, benefiting from a uniform and dense microporous structure and reinforced cell walls, exhibit superior structural rebound stability compared to the MPP system while maintaining a certain level of stiffness.[4]

The compression strength is a key parameter for assessing the ability of foam materials to resist external deformation. Fig. 9(a) shows the compression stress-strain curves of the samples at 80% strain. All the samples exhibited typical poly-

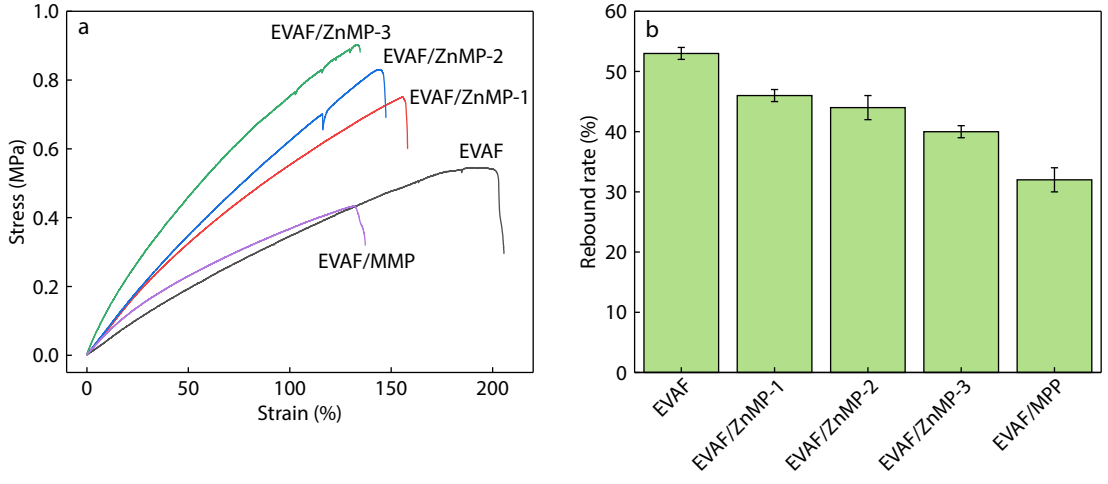


**Fig. 7** Stress-strain curves (a) and Rebound values (b) of EVAF, EVAF/ZnMP, and EVAF/MPP samples.

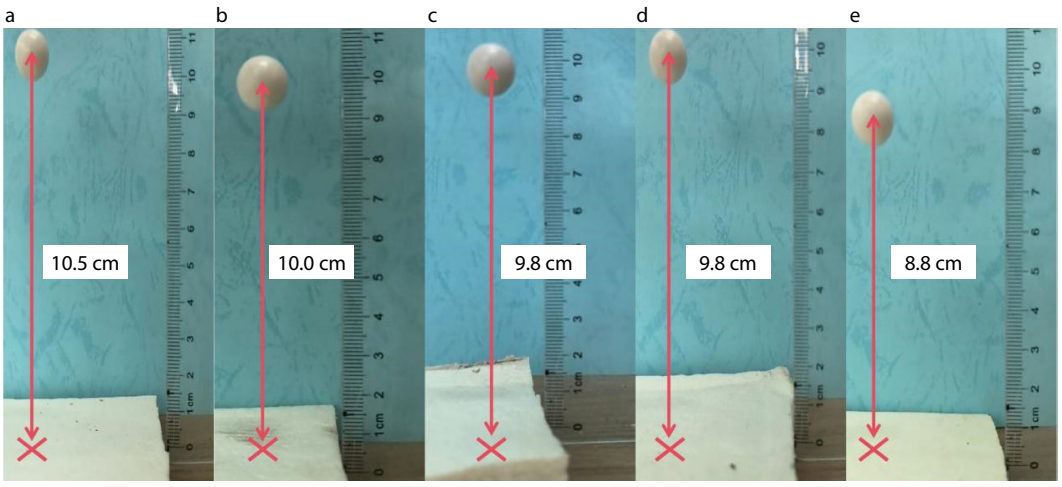


**Fig. 8** Rebound digital images of EVAF (a), EVAF/ZnMP-1 (b), EVAF/ZnMP-2 (c), EVAF/ZnMP-3 (d), and EVAF/MPP (e) samples.

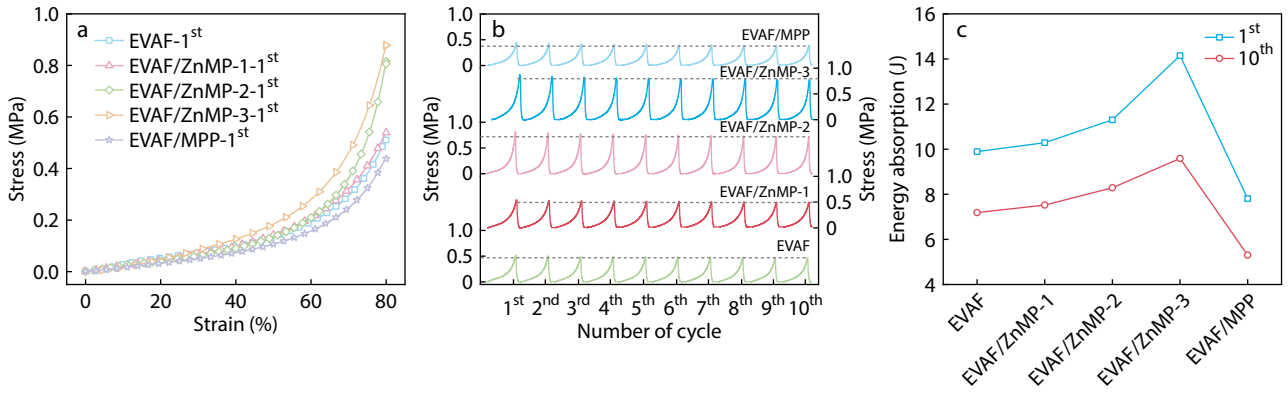


**Fig. 9** Compression curves (a), cyclic compression curves (b), energy absorption values (c) of EVAF, EVAF/ZnMP, and EVAF/MPP samples.

**Table 4** Foam density, specific tensile strength, specific compressive strength, and energy adsorption of EVAF, EVAF/ZnMP, and EVAF/MPP samples.

| Sample | Density ($g \cdot cm^{-3}$) | Specific tensile strength ($MPa \cdot cm^3 \cdot g^{-1}$) | Specific compressive strength ($MPa \cdot cm^3 \cdot g^{-1}$) | Specific energy adsorption ($J \cdot g^{-1}$) |
|---|---|---|---|---|
| EVAF | 0.28±0.02 | 1.93±0.16 | 1.82±0.14 | 1.962±0.141 |
| EVAF/ZnMP-1 | 0.30±0.01 | 2.50±0.12 | 1.83±0.10 | 1.906±0.060 |
| EVAF/ZnMP-2 | 0.31±0.03 | 2.68±0.26 | 2.61±0.26 | 2.025±0.201 |
| EVAF/ZnMP-3 | 0.33±0.01 | 2.73±0.17 | 2.67±0.17 | 2.382±0.073 |
| EVAF/MPP | 0.31±0.01 | 1.39±0.07 | 1.42± 0.17 | 1.400±0.051 |

mer foam compression behavior: linear elastic, plateau, and densification stages. Neat EVAF had a compression strength of 0.52 MPa. With the addition of ZnMP, the compression strength significantly increases, reaching 0.88 MPa for EVAF/ZnMP-3. This enhancement directly benefits from the microporous structure formed by the heterogeneous nucleation effect of ZnMP and the thickened cell walls (as seen in the SEM analysis), which markedly improves the load-bearing capacity of the cell skeleton. In comparison, compression strength of EVAF/MPP is only 0.44 MPa (Table S2 in ESI and Table 4), even lower than neat EVAF, indicating that the inferior cell structure severely weakens the material's compressive performance.[5] Based on the calculation of the specific energy absorption, the EVAF/ZnMP-3 sample exhibited the highest specific compressive performance, showing a 21.4% increase compared with neat EVAF. This result clearly demonstrates that ZnMPs significantly enhance the energy absorption capacity of the material.

To evaluate the reliability of the material for long-term use, 10-cycle compression tests (80% strain) were conducted (Figs. 9b and 9c). After 10 cycles, the compression strength retention rate is 91.06%, demonstrating good elastic recovery capability. The compression strength retention rate of EVAF/ZnMP-3 is 88.68%, which was slightly lower than that of neat EVA but still maintained high structural stability. This minor decline may be due to the high filler loading of the rigid particles, inducing partial microcracks during repeated large-deformation compression. However, the retention rate of EVAF/MPP is only 86.95% with the lowest absolute strength, confirming that the ZnMP system can maintain better mechanical integrity after multiple impacts and possesses excellent durability.[6]

These mechanical enhancements are consistent with zinc-embedded copolymers in PP, where interfacial improve-

ments yield an impact strength of 129% and a high cyclic retention.[7] Similar trends appear in hierarchical PU foams, with 253% compression boosting and reduced rebound for damping.[8] In nanocomposite SAN/PUA foams, nanodomains enable super-anti-compression and shape memory, mirroring the role of ZnMP in restricting chain slippage.[9] For sustainable PU foams, zeolite fillers achieve 7-fold strength gains with a stable rebound.[10] Balanced tensile/compression in EVAF/ZnMP outperforms unmodified IFR systems, addressing embrittlement *via* chelation.[1,11]

## Flame Retardancy and Mechanism Analysis

The limiting oxygen index (LOI) and vertical burning rating (UL-94) are the most intuitive indicators for evaluating the flame-retardant performance of a material. Table 5 summarizes the test results for different EVA foam materials. Neat EVAF is highly ignitable, burns intensely with severe melt dripping, fails to self-extinguish, has an LOI value of only 19.8% (a reference value based on typical pure EVA levels), and has no UL-94 rating.

With the addition of ZnMPs, the flame-retardant performance of the material significantly improved. At 10 wt% ZnMP, the LOI value increased to 24.7%, achieving a UL-94 V-1 rating. When the loading was increased to 15 wt% (EVAF/ZnMP-3), the LOI value further increased to 25.3% with a notably shortened self-extinguishing time, successfully passing the UL-94 V-0 rating. In contrast, the control sample with 10 wt% MPP (EVAF/MPP) only achieved V-1 rating. This indicates that the introduction of $Zn^{2+}$ significantly enhances the flame-retardant efficiency of the phosphorus-nitrogen system, enabling superior flame-retardant ratings at lower loadings, primarily because the metal ions promote the formation of a more stable char layer, effectively suppressing melt dripping.[12]

**Table 5** LOI and UL-94 test results of EVAF, EVAF/ZnMP, and EVAF/MPP samples.

| Sample | LOI (%) | Dropping | UL-94 |
|---|---|---|---|
| EVAF | 19.8 | Yes | None rate |
| EVAF/ZnMP-1 | 23.0 | Yes | V-2 |
| EVAF/ZnMP-2 | 24.7 | Yes | V-1 |
| EVAF/ZnMP-3 | 25.3 | No | V-0 |
| EVAF/MPP | 23.8 | Yes | V-2 |

Cone calorimetry testing simulates the combustion behavior in real fire scenarios. Fig. 10 shows the heat release rate (HRR) and total heat release (THR) curves for each sample, with the detailed data listed in Table 6.

### *Heat release behavior*

Neat EVAF shows an ignition time (TTI) of only 10 s and a peak heat release rate (PHRR) of 825.2 kW·m$^{-2}$. After the introduction of ZnMP, the TTI was extended to 18 s, indicating an enhanced ignition resistance. More importantly, EVAF/ZnMP-3's PHRR decreases to 486.6 kW·m$^{-2}$, a reduction of approximately 41.0% compared to neat EVAF. In terms of total heat release (THR), EVAF/ZnMP-3's THR value is only 37.9 MJ·m$^{-2}$, far lower than neat EVAF (91.5 MJ·m$^{-2}$) and EVAF/MPP (43.4 MJ·m$^{-2}$). The superior heat suppression effect of ZnMP over MPP confirms that the dense char layer catalyzed by $Zn^{2+}$ can more effectively block heat transfer, severing the energy feedback loop that sustains combustion.[13]

### *Smoke and toxicity analysis*

Smoke release is the primary cause of fire fatalities. As shown in Figs. 10(c) and 10(d) and Table 6, although the addition of flame retardants typically increases the total smoke production (TSP) owing to the promotion of incomplete combustion, the ZnMP system exhibits a relatively excellent smoke suppression potential. The TSP of EVAF/ZnMP-3's TSP is 11.02 m$^2$, which was significantly lower than EVAF/MPP's 12.59 m$^2$. Additionally, the CO

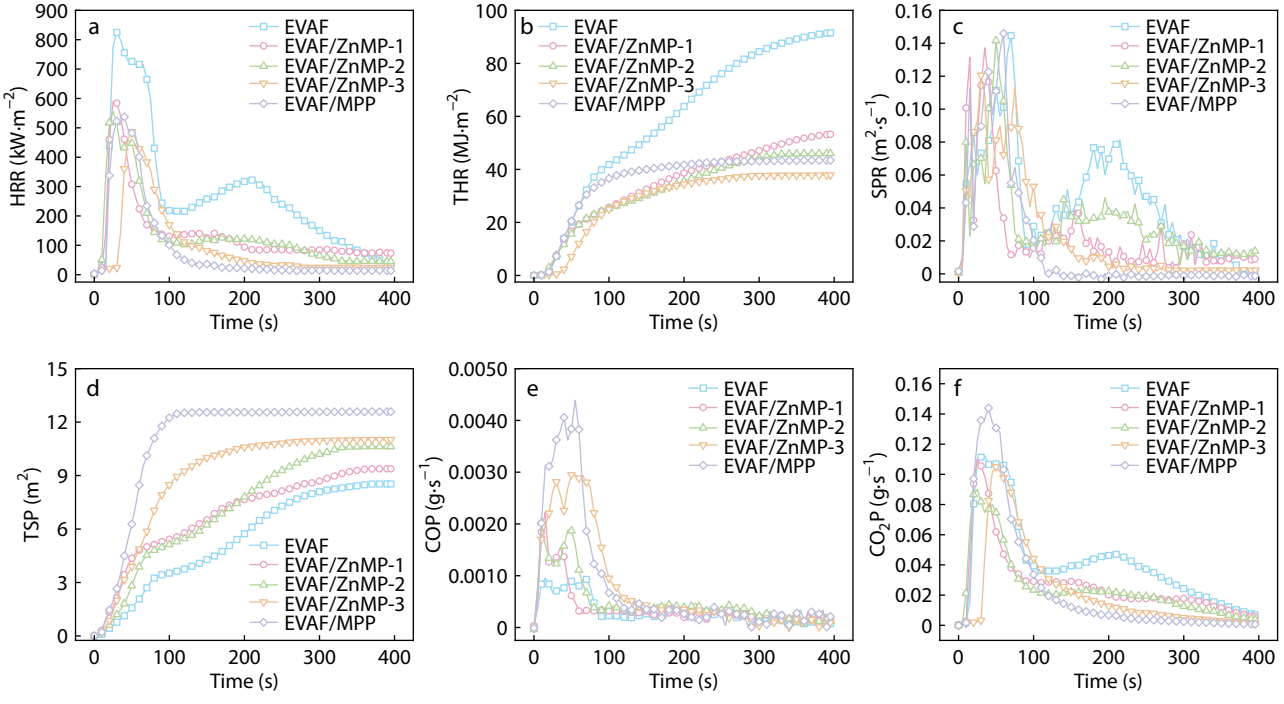


**Fig. 10** HRR (a), THR (b), SPR (c), TSP (d), COP (e), and $CO_2P$ (f) curves of EVAF, EVAF/ZnMP, and EVAF/MPP samples.

https://doi.org/10.1007/s10118-026-3672-z

**Table 6** Values of peak of HRR, THR, COP, and $CO_2P$ of EVAF, EVAF/ZnMP, and EVAF/MPP samples.

| Sample | pHRR (kW·m$^{-2}$) | THR (MJ·m$^{-2}$) | COP (g) | $CO_2P$ (g) |
|---|---|---|---|---|
| EVAF | 32.69 | 825.22 | 0.12 | 16.27 |
| EVAF/ZnMP-1 | 21.29 | 583.69 | 0.13 | 10.84 |
| EVAF/ZnMP-2 | 28.77 | 555.86 | 0.20 | 9.85 |
| EVAF/ZnMP-3 | 25.23 | 486.59 | 0.30 | 8.61 |
| EVAF/MPP | 19.74 | 537.69 | 0.28 | 9.42 |

and $CO_2$ production rate curves in Fig. 10 show that ZnMP addition substantially reduces the $CO_2$ yield (45.9% decrease for EVAF/ZnMP-3), while the CO yield increased slightly. This phenomenon is a typical feature of gas-phase radical trapping and condensed-phase char formation, indicating that ZnMP effectively disrupts complete oxidation reactions and retains more carbon in the condensed-phase char residue rather than converting them into gaseous emissions.[14]

To reveal the condensed-phase flame-retardant mechanism, the post-cone calorimetry char residues were analyzed using SEM and Raman spectroscopy. The SEM images (Fig. 11) show that neat EVAF leaves only a small amount of fragmented and loose char slag after combustion. In contrast, EVAF/ZnMP-3 formed a continuous, dense, and expanded "particle" char layer structure. This structure benefits from the zinc phosphate glass formed by $Zn^{2+}$ at high temperatures, which acts like "barrier" to protect the carbon skeleton and seal surface cracks.[15]

To further clarify the chemical composition of the residual char, XPS analysis was performed on the combustion residues (Fig. 12). The survey spectrum clearly shows the presence of Zn, P, O, C, and N, indicating that Zn-containing phosphate species remained in the condensed phase after combustion. In particular, the Zn 2p peaks observed at approximately 1021.5 eV (Zn 2p3/2) and 1044.6 eV (Zn 2p1/2) corresponded well to the zinc phosphate-type structures reported in the literature. Meanwhile, the P 2p signal centered at 133–134 eV is characteristic of phosphate species. These results suggest that during thermal decomposition, $Zn^{2+}$ interacts with phosphate groups to form thermally stable condensed-phase structures such as zinc phosphate glass and zinc pyrophos-

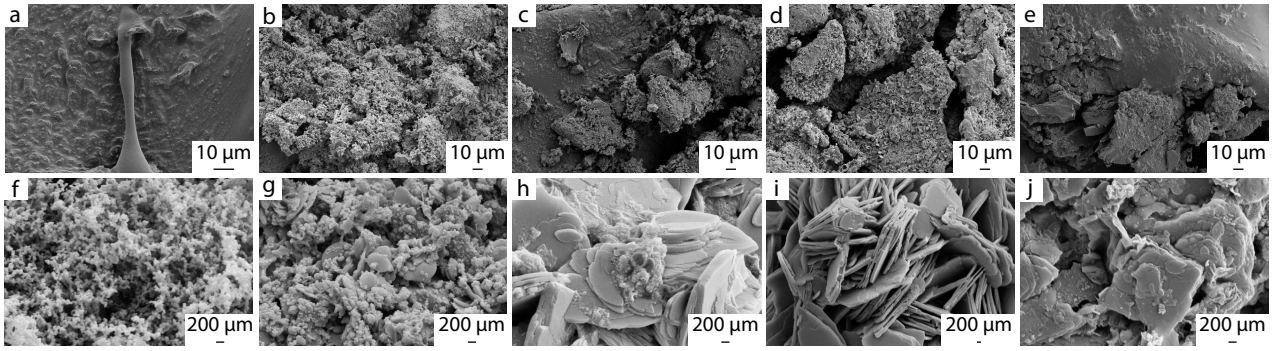


**Fig. 11** SEM images of char residues for different samples, arranged sequentially according to panel labels (a) to (j): (a–e) low-magnification SEM images of char residues, (f–j) corresponding high-magnification SEM images. Specifically, EVAF is displayed in (a, f), EVAF/MPP in (b, g), EVAF/ZnMP-1 in (c, h), EVAF/ZnMP-2 in (d, i), and EVAF/ZnMP-3 in (e, j).

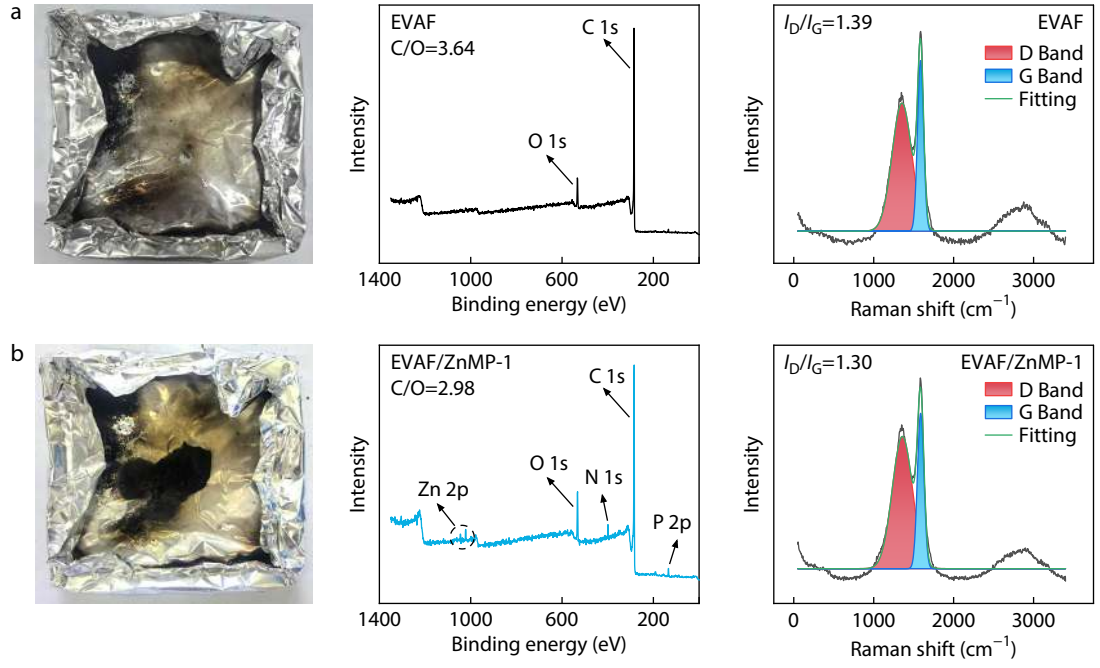

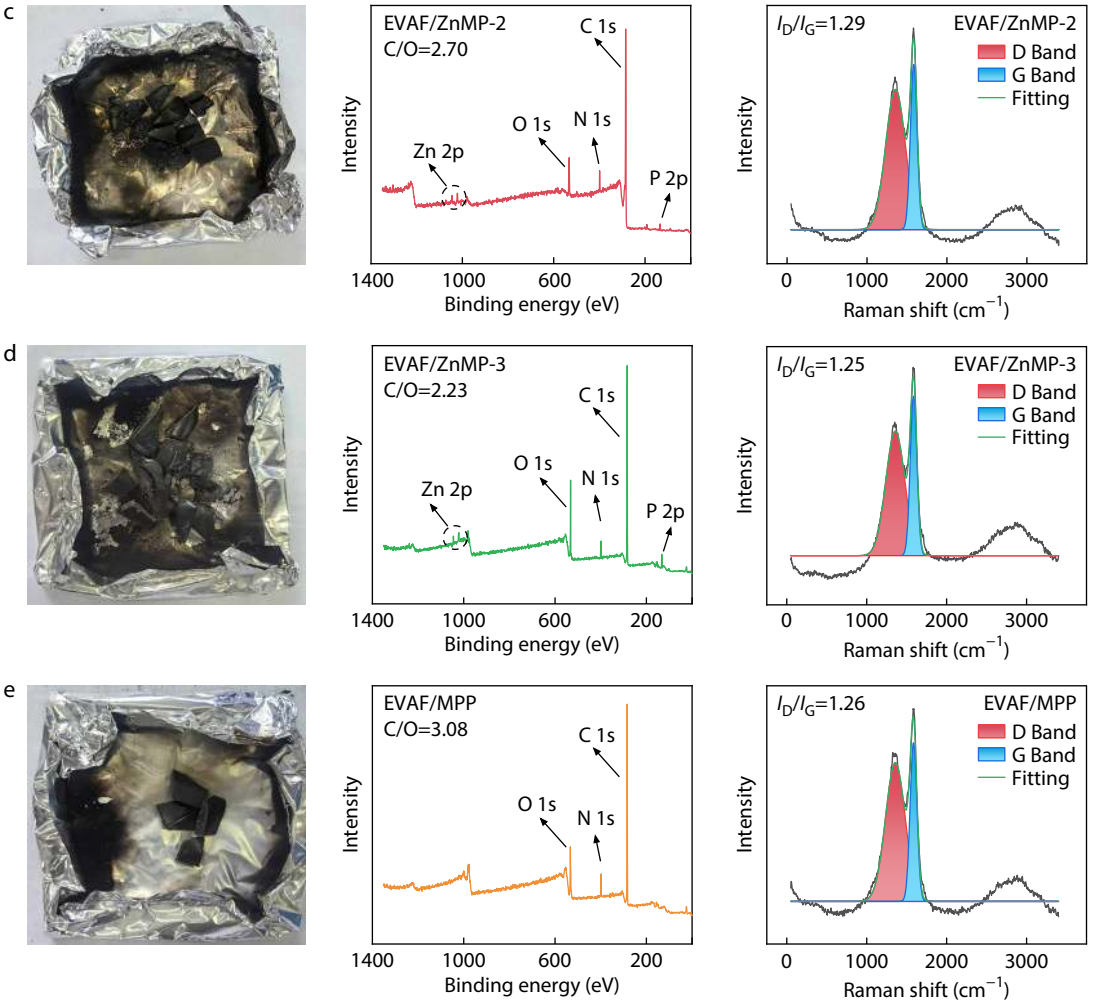


**Fig. 12** Char residue images, C1s spectra and Raman spectra of EVAF (a), EVAF/ZnMP-1 (b), EVAF/ZnMP-2 (c), EVAF/ZnMP-3 (d), and EVAF/MPP (e) samples.

phate. Such inorganic phosphate networks can act as rigid frameworks within the char layer, improving its structural integrity and thermal stability. This interpretation is consistent with the DTG results, where a reduced maximum weight-loss rate was observed for ZnMP-containing systems, indicating that the formation of these inorganic phosphate structures effectively stabilized the char during high-temperature degradation.

Raman spectroscopy (Fig. 12) was used to quantify the char quality. The intensity ratio of the D band (disordered carbon) to the G band (graphitic carbon) ($I_D/I_G$) is commonly used to evaluate the degree of graphitization of char residues.[10] EVAF/ZnMP-3 exhibits an $I_D/I_G$ value of 1.25, which decreases from 1.39 for neat EVAF and is slightly lower than that of EVAF/MPP (1.26). A lower $I_D/I_G$ value indicates that the char residue induced by ZnMP possesses a higher degree of structural ordering and forms a more compact carbon structure with improved thermal stability.[4,9] These graphitized char layers provide superior thermal insulation and oxygen barrier capability, acting as effective physical barriers during combustion. The formation of this dense carbonaceous layer can significantly inhibit the heat transfer and restrict the oxygen diffusion to the underlying polymer matrix. Consequently, the combustion process was effectively suppressed, which is consistent with the reduced heat release intensity observed in the cone calorimetry results.[16]

To evaluate the flame-retardant performance of the ZnMP system in a broader research context, a comparison with previously reported Zn-containing flame retardants in polymer matrices was conducted, as summarized in Table S3 (in ESI). The EVAF/ZnMP-3 composite exhibited mechanical strength retention of 46.70% at a loading of 15 wt%, together with an LOI value of 25.3% and a THR reduction of 41.04%. In contrast, several reported Zn-based flame-retardant systems in polypropylene matrices show significant deterioration in their mechanical properties despite achieving higher LOI values, indicating that the incorporation of these flame retardants severely compromises the mechanical integrity of the polymer matrix.[3,7,8] Although most systems, such as EP/IFR/ZnO composites, achieve higher LOI values and greater THR reductions, they require significantly higher additive loadings (up to 33 wt%), which may negatively affect processability and material performance.[1] In comparison, the ZnMP system developed in this study achieves a balanced combination of flame-retardant efficiency and mechanical performance at a

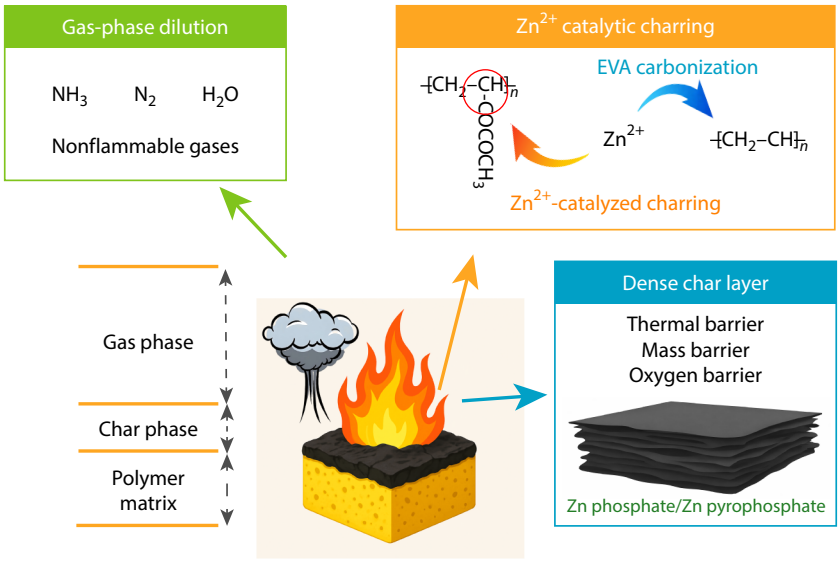


**Fig. 13** Proposed synergistic flame-retardant mechanism of ZnMP in EVA foams, including gas-phase dilution, $Zn^{2+}$-catalyzed charring, and formation of a dense organic–inorganic hybrid char layer.

relatively low additive loading.[12,13] This indicates that the coordinated Zn-containing structure can effectively enhance char formation and flame-retardant performance, while mitigating the mechanical deterioration typically associated with conventional flame-retardant additives.

## Mechanism Analysis

Based on the gas- and condensed-phase analyses, a synergistic flame-retardant mechanism of ZnMP in EVA foams was proposed, as illustrated in Fig. 13. Gas-phase dilution effect: during the initial combustion stage, the melamine groups in ZnMP thermally decompose to release nonflammable gases, such as $NH_3$ and $N_2$.[17] These gases dilute the combustible volatiles and oxygen around the flame zone, thereby suppressing flame propagation. Gas expansion facilitates the formation of an intumescent char layer.[18] Condensed-phase catalytic charring and barrier effect: $Zn^{2+}$ played a key catalytic role in the condensed phase. As a Lewis acid, $Zn^{2+}$ promotes dehydrogenation and crosslinking reactions of the EVA molecular chains, accelerating carbonization.[19] Simultaneously, the phosphate species generated during decomposition react with $Zn^{2+}$ to form thermally stable zinc phosphate and pyrophosphate structures. These inorganic species integrate with the carbonaceous matrix to form a compact organic–inorganic hybrid char layer, which effectively blocks heat transfer and oxygen diffusion. Structural reinforcement from heterogeneous nucleation: ZnMP acts as an efficient heterogeneous nucleating agent during foaming, leading to a refined and uniform microporous structure with thicker cell walls. This optimized cellular structure reduces the number of heat conduction paths and improves the structural integrity of the protective char layer, thereby contributing to improved flame retardancy. Overall, ZnMPs enhance the fire safety of EVA foams through a synergistic mechanism involving gas-phase dilution, condensed-phase catalytic charring, and structural reinforcement.

## CONCLUSIONS

This study proposes a synergistic strategy of "ion complexation-interfacial modification" to successfully prepare a silane coupling agent-modified zinc ion-reinforced melamine phosphate flame retardant (ZnMP), which was applied to fabricate high-performance EVA composite foams. The introduction of $Zn^{2+}$ plays a template-guiding role during synthesis, inducing preferential growth of melamine phosphate crystals along the (1 −1 1) plane and transforming their morphology from irregular large-sized lamellae to regular fine structures. After surface modification with a silane coupling agent, ZnMP exhibited excellent dispersibility in the EVA matrix and acted as an efficient heterogeneous nucleating agent, significantly refining the cell size and constructing a dense and uniform microporous structure. Benefiting from the enhanced interfacial interactions and optimized cell skeleton, the EVA/ZnMP composites exhibited excellent rigidity and compressive strength. The sample with 15 wt% ZnMP shows a storage modulus at −64.9 °C increased by 144.3% compared to neat EVA, with compressive strength elevated to 0.88 MPa, and maintains good structural integrity after 10 compression cycles. This sample passed the UL-94 V-0 flame retardant test with a limiting oxygen index (LOI) of 26.3%. Cone calorimetry and char residue analysis revealed multiple flame-retardant mechanisms of ZnMP. In the gas phase, the flame retardant decomposes to release non-combustible gases, diluting the fuel and oxygen concentrations, whereas in the condensed phase, $Zn^{2+}$ acts as a Lewis acid catalyst, promoting dehydrogenation and cross-linking of polymer chains, and inducing the formation of highly thermally stable zinc phosphate glass. This "organic-inorganic hybrid" dense char layer, combined with the barrier effect of the microporous structure on heat transfer, significantly reduces the heat release rate (PHRR decreased by 41.0%) and total heat release, effectively suppressing fire spread. In summary, the ZnMP flame retardant developed in this study not only addresses the issues of high loading and poor mechanical properties associated with traditional inorganic flame retardants but also provides a new design approach for developing advanced polymer foams with lightweight, high-strength, and high flame-retardant characteristics.

https://doi.org/10.1007/s10118-026-3672-z

## Conflict of Interests

The authors declare no interest conflict.

## Electronic Supplementary Information

Electronic supplementary information (ESI) is available free of charge in the online version of this article at http://doi.org/10.1007/s10118-026-3672-z.

## Data Availability Statement

The related data of this paper is data that should not be shared, and can be obtained from the author for reasonable reasons. The author's contact information: yyzheng@fzu.edu.cn.

## ACKNOWLEDGMENTS

This work was financially supported by the Fujian Provincial Science and Technology Program Project (No. 2025H6033) and Fujian Provincial Young and Middle-Aged Teachers' Education and Research Project (No. JAT241082), and Foundation for Cultivated Young Talents of Fujian Province, China (No. 2025350180).

## REFERENCES

1 Jia, P. F.; Yu, F. H.; Tao, Y. J.; Sun, P. F.; Xing, W. Y.; Jie, G. X.; Hu, Y.; Wang, B. B. Multifunctional additive: a novel regulate strategy for improving mechanical property, aging life and fire safety of EVA composites. *Chem. Eng. J.* **2023**, *473*, 145283.
2 Mei, G. L.; Wang, S.; Li, Z. M.; Wang, W. H.; Hu, Z. H.; Hu, Y.; Gong, X. L. Flame-retardant, lightweight, and multiple safeguarding fire alarm sponge for firefighter safety detection. *Chem. Eng. J.* **2025**, *513*, 162905.
3 Shi, X. F.; Shi, F.; Luo, C. Z.; Zhang, C. H.; Shang, L. Bio-based phosphorus multifunctional P/N flame retardant to improve synergistically the mechanical and fire resistance of epoxy resin. *Mater. Today Chem.* **2025**, *46*, 102755.
4 Tian, M.; You, J. G.; Qiu, J.; Li, M. G.; Xing, H. P.; Xue, J.; Jiang, Z. W.; Tang, T. Unexpected super anti-compressive styrene-acrylonitrile copolymer/polyurea nanocomposite foam with excellent solvent resistance, re-processability and shape memory performance. *Compos. Part B-Eng.* **2023**, *264*, 110908.
5 Zhang, Y. M.; Qian, L. J.; Wang, J. Y.; Qiu, Y.; Xi, W. A zinc-embedded multicomponent copolymer customized for polypropylene and its synergistic flame-retardant effect and outstanding mechanical properties. *Polym. Degrad. Stabil.* **2024**, *224*, 110762.
6 Shorten, M. R. Energy return in footwear–revisited. *Footwear Sci.* **2024**, *16*, 149–162.
7 Pascarella, A.; Recupido, F.; Lama, G. C.; Sorrentino, L.; Campanile, A.; Liguori, B.; Berthet, M.; Rollo, G.; Lavorgna, M.; Verdolotti, L. Design and development of sustainable polyurethane foam: A

## Graphical Abstract

**Construction of Zinc Ion-reinforced Melamine Phosphate Flame Retardant for Synergistic Enhancement of Flame Retardancy and Energy Absorption in Ethylene-Vinyl Acetate Foams**

Xian-Sheng Hong and Yu-Ying Zheng

*Fuzhou University; Fujian Polytechnic Normal University*

Zinc ion chelated melamine phosphate (MPP) optimizes pore structure and forms a dual-phase barrier, significantly enhancing foam energy absorption and flame retardancy *via* combined gas and char reinforcement.

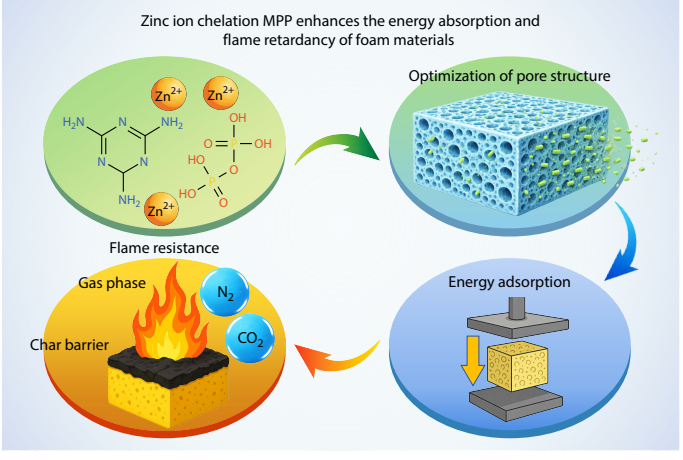

proof-of-concept as customizable packaging for cultural heritage applications. *Adv. Eng. Mater.* **2024**, *26*, 2301888.
8 Zhao, G.; Wang, H. M.; You, J. G.; Xing, H. P.; Xue, J.; Jiang, Z. W.; Tang, T. Superlight flame-retardant poly(aryl ether ketone)/polyurea nanocomposite foam with excellent solvent-resistance and shape memory performance. *Compos. Commun.* **2024**, *48*, 101946.
9 Shi, Y. Q.; Wu, S. J.; Chen, J.; Tang, L. C.; Gao, J. F.; Zou, H. F.; Song, P. A.; Qiu, T. Hierarchically building flame retardant and flexible electromagnetic interference shielding composites with tunable mechanism. *J. Mater. Sci. Technol.* **2025**, *239*, 39–54.
10 Mueller, P.; Schartel, B. Melamine poly(metal phosphates) as flame retardant in epoxy resin: performance, modes of action, and synergy. *J. Appl. Polym. Sci.* **2016**, *133*, 43549.
11 Liu, H.; Xu, W. X.; Ren, H. Z.; Li, D. X.; He, J. M.; Xia, L.; Xu, Y. T.; Zeng, B. R.; Yuan, C. H.; Dai, L. Z. Integrated comprehensive protection coating achieved by ligand engineering modulated MXene@LDH heterojunction with anti-corrosion, electromagnetic wave absorption and fire safety. *Chem. Eng. J.* **2024**, *486*, 150444.
12 Maou, S.; Meftah, Y.; Olmosovich Khakberdiev, E.; Grohens, Y. Thermal and viscoelastic behaviors of recycled polyvinyl chloride/styrene-acrylonitrile blend composites incorporating treated date palm fibers. *J. Thermoplast. Compos. Mater.* **2025**, DOI:10.1177/08927057251403504.
13 Song, Z. M.; Zhang, S. H.; Yu, X. L.; Hong, N. N.; Jia, P. F.; Xu, J. Y.; Cao, H. Z.; Han, D. Q.; Hu, Y.; Zhou, S.; Wang, B. B.; Gui, Z. Rare-earth-based hybrid flame retardant for EVA composites: flame-smoke-mechanical synergistic design. *Polym. Degrad. Stabil.* **2025**, 111586.
14 Liu, D.; Huyan, C. X.; Li, H. X.; Ge, J.; Chen, F.; Zhang, L. Q. Recycling and upcycling of polyurethane thermosets: the second life of polymers. *Adv. Mater.* **2026**, *38*, e15809.
15 Fan, T.; Xue, S. S.; Zhu, W. B.; Zhang, Y. Y.; Li, Y. Q.; Chen, Z. K.; Huang, P.; Fu, S. Y. Multifunctional polyurethane composite foam with outstanding anti-impact capacity for soft body armors. *ACS Appl. Mater. Interfaces* **2022**, *14*, 13778–13789.
16 Yin, Z. T.; Chu, F. K.; Yu, B.; Wang, B. B.; Hu, Y. Hierarchical $Ti_3C_2T_x$@BPA@ PCL for flexible polyurethane foam capable of anti-compression, self-extinguishing and flame-retardant. *J. Colloid Interface Sci.* **2022**, *626*, 208–220.
17 Liu, X. L.; Zhu, M. H.; Zhu, J. H.; Liu, Z. H.; Geng, Y. W.; Xie, C. X.; Chen, X. L.; Liu, L.; Song, P. A. A ceramifiable organic-inorganic fire extinguishing hybrid coating capable of cyclic fire-warning. *Polym. Degrad. Stabil.* **2025**, *234*, 111208.
18 Zhang, J. H.; Wang, X.; Tan, L. C.; Wang, Q. Y.; Yu, H. W.; Xu, W. H.; Xu, B. P.; Xiao, S. P.; Huang, J. R. A facile toughening strategy for styrene–acrylonitrile copolymer through dynamic vulcanization of acrylonitrile-butadiene rubber. *J. Appl. Polym. Sci.* **2026**, *143*, e57992.
19 Orabona, F.; Recupido, F. Cutting-edge development of non-isocyanate polyurethane (NIPU) foams: from sustainable precursors to environmental impact evaluation. *Green Chem.* **2025**, *27*, 7403–7444.